ELSEVIER

20 June 1997

Chemical Physics Letters 272 (1997) 48–54

CHEMICAL PHYSICS LETTERS

Intrinsic optical heterodyne detection of a two-dimensional fifth order Raman response

Andrei Tokmakoff, Matthew J. Lang, Delmar S. Larsen, Graham R. Fleming

Department of Chemistry and the James Franck Institute, University of Chicago, 5735 S. Ellis Ave., Chicago, IL 60637, USA

Received 4 April 1997

Abstract

Intrinsic optical heterodyne detection is applied to femtosecond two-dimensional (2-D) vibrational spectroscopy of the Raman active inter- and intramolecular modes of liquid CS_2 between 1 and 1000 cm^{-1}. Heterodyne detection is accomplished with a novel wave vector matching geometry that allows detection of the cross term between the third and fifth order response, $R^{(3)}R^{(5)}$. The increase in the bandwidth and sensitivity through this detection technique will allow the measurement of 2-D temporal or spectral responses for a wide variety of systems in this frequency range. © 1997 Elsevier Science B.V.

1. Introduction

Fifth order nonresonant Raman spectroscopy has received considerable attention recently as a probe of the microscopic dynamics of condensed phases. This two-dimensional (2-D) optical rephasing technique has been shown to be sensitive to heterogeneous dynamics in condensed phases [1–3]. These predictions have led to a number of experiments to quantify microscopic variations in the intermolecular dynamics of neat CS_2 [4–9], and liquid mixtures with CS_2 [10]. Further theoretical work has demonstrated the sensitivity of this experiment to anharmonicity in intermolecular vibrations [11,12]. In addition, fifth order Raman experiments have allowed experimental probing of the dephasing of high frequency vibrational overtones [13].

As with other optical echo spectroscopies, a distribution of dynamics within the ensemble can be observed by the constructive interference between the individual microscopic responses along the diagonal time axis in the 2-D temporal response [1–3,9,14]. In practice thus far such effects are small; however, the full temporal 2-D Raman response has been shown to be sensitive to the microscopic details of the liquid dynamics [9]. It is also clear that an extension of these experiments to the study of intramolecular dynamics can give direct information on the coupling between well defined vibrational degrees of freedom.

The five field interaction sequence for the nonresonant fifth order experiment is shown in Fig. 1a. A vibrational coherence is created by excitation with a pair of Raman excitation fields at time $t_0 = 0$. The coherence evolves for a time $\tau_2 = t_2 - t_0$ at which point a second pair of Raman fields induce certain rephasing processes. The evolution of the coherence after the second period $\tau_4 = t_4 - t_2$ is probed by scattering a probe pulse E_5 off the coherence, generating a polarization P. Tanimura and Mukamel orig-

PII S0009-2614(97)00479-X

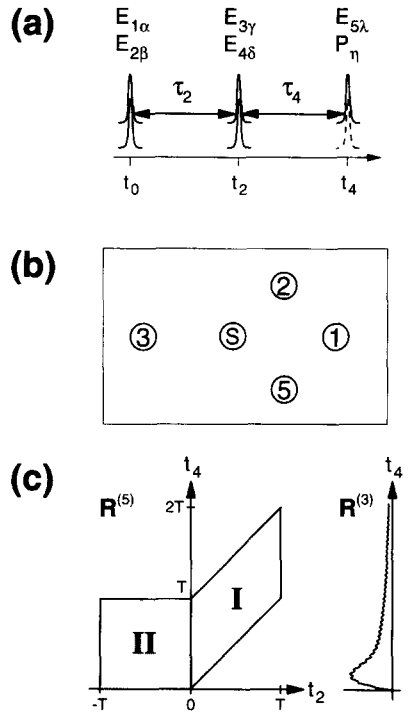

Fig. 1. (a) Time variables in the nonresonant fifth order Raman experiment. $\alpha-\eta$ refer to the polarization of the input beams. (b) The heterodyned fifth order wave vector matching geometry, showing the cross-section of the beams and signal (circled S) perpendicular to the direction of propagation. In the heterodyne configuration both the E_3 and E_4 interactions are derived from pulse (circled 3). (c) The temporal regions of fifth order signal generation (I and II) for the two time dimensions given in (a), as dictated by causality and the symmetry to pulse interchange. Also shown is the time axis for decay of the cross term third order signal.

inally showed that the fifth order polarization can be described by three-point Raman polarizability correlation functions in the form [1]

$$\overline{R}^{(5)}(\tau_2,\tau_4) = \frac{1}{\hbar^2}\langle[[\bar{\alpha}(t_4),\bar{\alpha}(t_2)],\bar{\alpha}(t_0)]\rangle, \tag{1a}$$

$$= -\frac{1}{\hbar^2}\langle[[\bar{\alpha}(\tau_4+\tau_2),\bar{\alpha}(\tau_2)],\bar{\alpha}(0)]\rangle. \tag{1b}$$

Note that the fifth order response is a sixth rank tensor quantity given by the three point interaction with the second rank Raman polarizability tensor for the system. While this expression is general for any nonresonant fifth order Raman experiment, in the following we study the degenerate six-wave mixing signal of the Raman active modes within the bandwidth of fs excitation pulses (1–1000 cm^{-1}).

Most of the experimental difficulty with fifth order Raman spectroscopy lies in the detection. The weak rephasing pathway of the fifth order signal must be distinguished from non-rephasing fifth order signals, hyperpolarizability contributions, much stronger third order signals, the fundamental beams, and scattered light. These problems have led to the design of selective wave vector matching geometries for the homodyne detected signal [5,8,9]. The generation of a unique direction for the true 2-D fifth order signal requires the use of five independent pulses [9]. Even with a selective homodyne detection geometry, microjoule level pulse energies are required to observe responses in even the most polarizable samples, with intensities approaching the threshold for continuum generation.

In order to increase the sensitivity of detection it is desirable to implement optical heterodyne detection of the fifth order signal [15,16]. This phase sensitive technique has the further advantage that the signal generated is linearly proportional to the nonlinear response, rather than the modulus squared homodyne response. Heterodyne detection of third order nonlinearities is most often accomplished by intrinsic heterodyne detection, in which the signal is generated in the same wave vector matching direction as the probe beam [16]. In this geometry the probe beam that generates the signal also acts as a phase-locked local oscillator field, and the detector observes the intensity of the sum of the probe and signal fields. By chopping the pump beam, the dominant probe beam contribution to the signal can be eliminated yielding a signal that is effectively proportional to the third order response

$$I(t) = \frac{nc}{4\pi}\left[|E_{\mathrm{LO}}(t)+R^{(3)}(t)|^2 - |E_{\mathrm{LO}}(t)|^2\right]$$

$$\approx \frac{nc}{2\pi}\mathrm{Re}\left[E^*_{\mathrm{LO}}(t)\cdot R^{(3)}(t)\right], \tag{2}$$

when $E_{\mathrm{LO}} \gg R^{(3)}$. Intrinsic heterodyne detection experiments include virtually every resonant or nonresonant third order pump–probe experiment. Other heterodyne detection techniques of third order signals have more flexibility in selecting the tensor element to be observed, but generally require signifi-

cant effort in introducing or characterizing the local oscillator, or in signal detection. These include a phase-locked Mach–Zehnder interferometer [17], position sensitive Kerr lens spectroscopy [18,19], and heterodyning between the nuclear response and an accumulated thermal grating [20].

Intrinsic heterodyne detection of the fifth order Raman signal cannot be accomplished by choosing a wave vector matching geometry that generates the fifth order signal collinear with the final probe pulse E_5, since there are necessarily far stronger third order signals generated in the same direction. Instead we use the third order signal as the intrinsic local oscillator field and generate the fifth order signal along the same wave vector matching direction with the addition of one additional pump beam from which the E_3 and E_4 interactions are derived. Fig. 1b shows the wave vector matching geometry chosen for this experiment. A nonresonant third order signal $R^{(3)}_{\xi\lambda\beta\alpha}(t_4)$ with wave vector matching direction $k_S = k_5 + k_2 - k_1$ is generated in a box grating geometry by the time-coincident Raman excitation pulse pair $E_{1\alpha}$ and $E_{2\beta}$ and the probe beam $E_{5\lambda}$. A Raman interaction with an additional pump pulse ($E_{3\gamma}E^*_{3\gamma}$) incident at time t_2 prior to $E_{5\lambda}$ generates the fifth order signal $R^{(5)}_{\eta\lambda\gamma\gamma\beta\alpha}(t_2, t_4 - t_2)$ along the same wave vector matching direction $k_S = k_5 + (k_3 - k_3) - (k_1 - k_2)$. By chopping the pump beam and detecting the change in the third order signal, we can detect the cross term between the third and fifth order response

$$I(\tau_2,\tau_4) \propto |R^{(3)}_{\xi\lambda\beta\alpha}(t_4) + R^{(5)}_{\eta\lambda\gamma\gamma\beta\alpha}(t_2, t_4 - t_2)|^2 - |R^{(3)}_{\xi\lambda\beta\alpha}(t_4)|^2, \quad (3a)$$

$$\approx 2\mathrm{Re}\left[R^{(3)}_{\xi\lambda\beta\alpha}(\tau_2+\tau_4) \cdot R^{(5)}_{\eta\lambda\gamma\gamma\beta\alpha}(\tau_2,\tau_4)\right], \quad (3b)$$

if the amplitude of $R^{(3)} \gg R^{(5)}$. Here and in the following, references to the time variables associated with $R^{(5)}(\tau_2, \tau_4)$ refer respectively to the time intervals of the correlation function ($\tau_i \geqslant 0$). Knowing the third order response, which can be measured by nonresonant pump–probe, optical-heterodyne-detected Raman-induced Kerr effect spectroscopy (OHD-RIKES), or the other heterodyne techniques mentioned above, allows the fifth order response to be extracted. Likewise the cross term in Eq. 3b can be modeled directly in interpreting the 2-D response.

The 2-D signal described above is generated for the condition $t_4 > t_2 > 0$, which is pictured as Region I in Fig. 1c. In addition, a fifth order signal also exists for $t_4 > 0 > t_2$ due to the pulse exchange symmetry between the Raman pulse pair $E_{1\alpha}E^*_{2\beta}$ and the Raman pair derived from pulse 3, $E_{3\gamma}E^*_{3\gamma}$. In this case, pictured by Region II in Fig. 1c, the fifth order signal $R^{(5)}_{\eta\lambda\beta\alpha\gamma\gamma}(-t_2, t_4)$ is generated in the same wave vector matching direction as the third order signal

$$I(\tau_2,\tau_4) \propto |R^{(3)}_{\xi\lambda\beta\alpha}(t_4) + R^{(5)}_{\eta\lambda\beta\alpha\gamma\gamma}(-t_2, t_4)|^2 - |R^{(3)}_{\xi\lambda\beta\alpha}(t_4)|^2, \quad (4a)$$

$$\approx 2\mathrm{Re}\left[R^{(3)}_{\xi\lambda\beta\alpha}(\tau_4) \cdot R^{(5)}_{\eta\lambda\beta\alpha\gamma\gamma}(\tau_2, \tau_2+\tau_4)\right]. \quad (4b)$$

Eq. (4) demonstrates that full symmetry to the interchange of the pulses does not exist in the detection of the $R^{(3)}R^{(5)}$ cross term. Since the third order signal decays in the t_4 time dimension, it damps the 2-D signal in Region I in both time dimensions, but only damps the τ_4 dimension in the Region II signal.

2. Experimental

We demonstrate the fifth order heterodyne technique by obtaining the fifth order response $R^{(5)}_{zzzzzz}$ from liquid CS_2 which probes the modes of the polarized Raman spectrum [21]. The full 2-D homodyne response for this fifth order signal has been previously characterized with 60 fs pulses [9]. The data shown here was collected with two bandwidths. Broad bandwidth measurements were taken with 27 fs pulses, which allowed observing the inter- and intramolecular response of CS_2, while narrow bandwidth measurements with 45 fs pulses were sensitive only to the intermolecular response.

For broad bandwidth measurements, the response was measured with amplified pulses derived from a cavity-dumped Ti:sapphire oscillator [22]. Pulses of 35 nJ, dumped at a repetition rate of 3.8 kHz, were amplified in a double-pass Z-fold amplifier constructed of two 10 cm radius of curvature mirrors about a 4 mm Brewster-cut Ti:sapphire crystal. Pumping the amplifier with 1 mJ, 400 ns pulses from a frequency doubled Q-switched Nd:YLF, yielded 750 nJ pulses with 45 nm bandwidth ($\lambda = 785$ nm).

Prism compression yielded 27 fs sech^2 pulses with 130 nJ total energy at the sample. Narrower bandwidth data were taken with 45 fs sech^2 pulses obtained by 3.8 kHz regenerative amplification of the Ti:sapphire oscillator pulses [23]. Microjoule level energies were available at the sample with this system.

The beams were split in a manner similar to the arrangement in Ref. [9]. The energy in beams 1, 2, 3, and 5 was split in a ratio of 1:1:2:1, respectively. Two stepper motor translation stages allowed the timing of pulses 3 and 5 relative to the pulse pair 1 and 2. In all cases, the polarization of all beams were parallel, implying that the $R^{(5)}_{ZZZZZZ}$ tensor component was measured. The beams were focused into the sample in the wave vector matching geometry of Fig. 1b. For the 27 fs data, an 8 cm achromatic doublet was used to focus to a spot size of 50 μm at the sample, whereas the 45 fs data were taken by focusing with a 30 cm singlet to 270 μm. The third order signal $k_S = k_5 + k_2 - k_1$ and the superimposed fifth order response were detected with a Si photodiode, amplified ten times, and sampled with a gated integrator. The $R^{(3)}R^{(5)}$ cross term was extracted by chopping beam 3 at 1.9 kHz and detecting the gated integrator output with a lock-in amplifier. Data was taken in Region II of Fig. 1c, by stepping in 6.67 fs steps in both time dimensions. Scans along t_2 were averaged before stepping in the t_4 direction, with a total collection time of $\approx$ 30 h for the 27 fs data and $\approx$ 12 h for the 45 fs data. The integrity of the data set was checked by comparison of cross scans along t_4 at several t_2 intervals with the corresponding slices from the data matrix.

3. Results and discussion

Fig. 2 shows the 1-D third order polarized Raman response of liquid CS_2 taken with 27 fs pulses. The data presented is the square root of the homodyne signal, $\sqrt{|R^{(3)}_{ZZZZ}(\tau)|^2}$. Other than the superior signal to noise ratio, there is no difference between the data in Fig. 2 and the third order intrinsic heterodyne response obtained with a simple nonresonant pump–probe experiment (see Eq. (2)). The data show the inertial rise of intermolecular dynamics, peaking at $\tau = 150$ fs, and then damping to diffusive behavior. On longer time scales the data approaches exponential damping with a time constant of 1.6 ps, as expected for $\tau > 2$ ps [8,24]. These low frequency dynamics are indistinguishable from the dynamics observed in the depolarized response of CS_2 measured with OHD-RIKES [8,24]. The $R^{(3)}_{ZZZZ}$ response is also modulated by beating from the impulsive excitation of the 654 cm^{-1} ν_1 symmetric S=C=S stretching mode. The imaginary Fourier transform spectrum of a fit to this response, after removal of the hyperpolarizability spike at $\tau = 0$, is also shown, emphasizing the clear separation of inter- and intramolecular modes.

Fig. 3 shows the 2-D response of the cross term $R^{(3)}(\tau_4) \cdot R^{(5)}(\tau_2, \tau_4)$ of CS_2 taken with 27 fs pulses and filtered to remove frequency components above 230 ps^{-1} (1200 cm^{-1}). The contour plot shows the general features of the response, which bear similarity to those of the homodyne response [9]. The 2-D signal peaks at $\tau_2 = \tau_4 \approx 150$ fs and decays rapidly along the diagonal. Ridges along $\tau_i = 150$ fs are observed in both dimensions, corresponding to the peak of the inertial component in the third order response. The rate of decay along τ_2, which follows the diffusive response at long time, is distinctly slower than along τ_4 [9,14]. As seen in the surface plot, the signal is modulated in both dimensions by the intramolecular dynamics. The strong signals along the time axes arise from 1-D hyperpolarizability contributions to the fifth order signal; these have been discussed previously [9,14].

The spectral representation of the 2-D cross-term response is shown in Fig. 3 by the absolute value

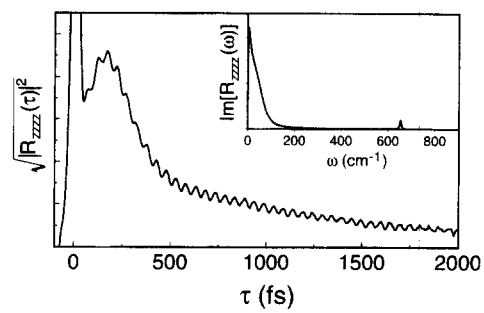

Fig. 2. The third order R_{ZZZZ} response from CS_2, obtained from the square root of the homodyne signal. The imaginary part of a multimode fit to the Fourier transform of the time domain data is shown in the inset.

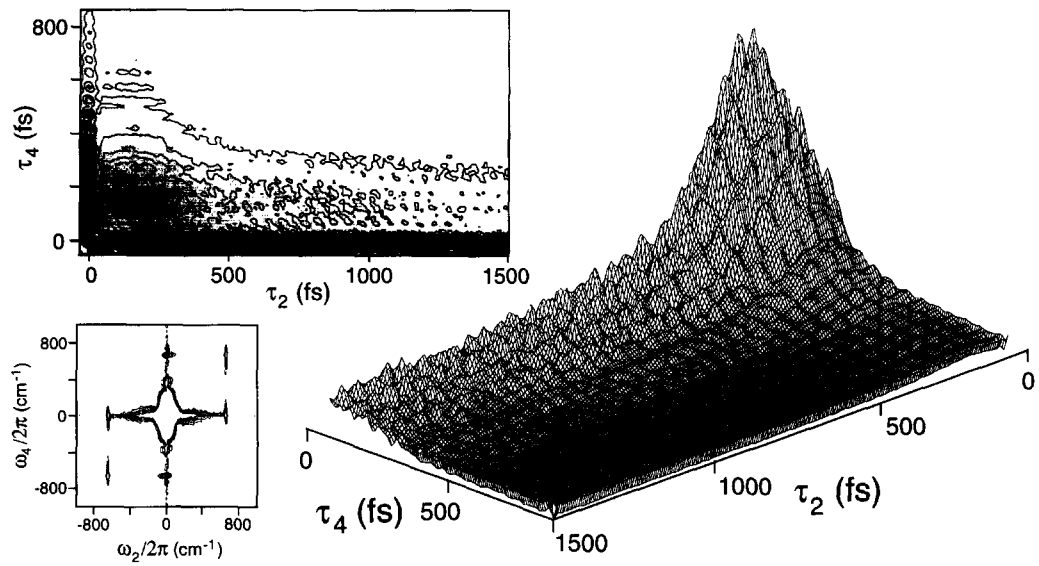

Fig. 3. Heterodyne 2-D Raman response, $R^{(3)}_{ZZZZ}(\tau_4)R^{(5)}_{ZZZZZZ}(\tau_2,\tau_4)$, of CS_2. The contour plot shows features in 10% contours relative to the 2-D signal maximum. The surface plot, with hyperpolarizability contributions truncated, shows the modulation due to the ν_1 mode of CS_2. The absolute value 2-D Fourier transform of the time domain data, shown in the lower left, shows contours from 6% to 14% of maximum in 2% intervals.

2-D Fourier transform of the time domain data. The spectrum shows the strong intermolecular peak centered at zero frequency and the diagonal peaks of the ν_1 mode at $\omega_2 = \omega_4 = \pm 653$ cm^{-1}. The diagonal frequency slice that contains these peaks is the equivalent of the 1-D observable [25]. The elongated shape of these peaks along ω_4 is partially due to the decay of the third order response along τ_4 in the cross term. In addition, strong cross peaks are observed between the inter- and intramolecular modes. The existence of cross peaks is considered a sign of coupling between the dynamics of the corresponding diagonal frequency components [25]. With reference to the techniques developed with 2-D NMR, it is likely that analysis of the details in such spectra will lead to an enhanced understanding of the molecular motions involved in the dynamics of liquids.

Fig. 4 shows three tests that determine uniquely that the true 2-D fifth order heterodyne signal is measured. In Fig. 4a, the full fifth order heterodyne response taken with 45 fs pulses in both Regions I and II is shown. The response shows the correct shape predicted by Fig. 1c. Further, the long time decay rate along the positive diagonal $t_2 = t_4$ (Region I) is twice as fast as the decay along $-t_2$ (Region II). Fig. 4b shows the decay along $-t_2$ for $t_4 = 100$ fs taken with 27 fs pulses, which on ps time scales approaches an exponential decay with a 1.6 ps time constant. This observation indicates a response that is linearly proportional to $R^{(5)}$, and thus a heterodyned signal as predicted by Eq. 4. A homodyne signal would be expected to decay with a 0.8 ps time constant [8,9]. A final test of a true heterodyned response comes from a power dependence of the $R^{(3)}R^{(5)}$ cross term signal intensity, which is expected to scale as the fourth power of the total incident intensity. The power dependence shown in Fig. 4c confirms this prediction over > 4 decades of signal intensity.

For previous 1-D nonresonant intrinsic heterodyne experiments, i.e. OHD-RIKES [26], the polarization geometry has been chosen to allow the magnitude of the local oscillator to be adjusted within an order of magnitude of the third order signal level. This is done by rotating the polarization of the incoming probe beam to be approximately crossed with the probe beam analyzing polarizer. The slight mismatch allows a much attenuated part of the probe beam to be introduced as the local oscillator. Specifically, $\varphi_1 = \varphi_2 = 0°$, $\varphi_3 \approx 45°$, $\varphi_4 = -45°$, where φ_i are

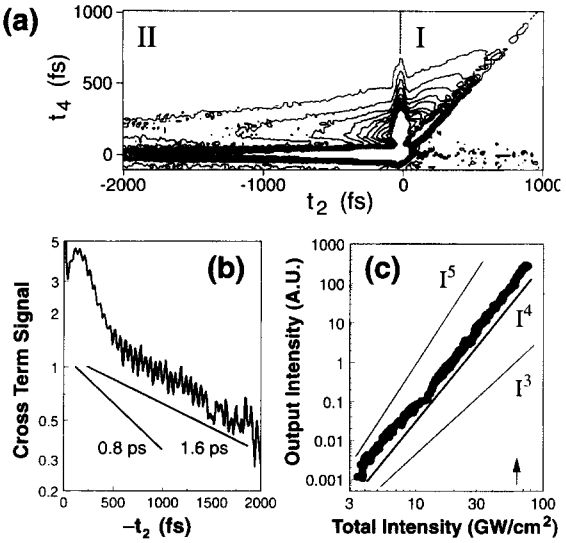

Fig. 4. Characterization of the heterodyned fifth order Raman experiment. (a) $R^{(3)}_{ZZZZ}R^{(5)}_{ZZZZZZ}$ response of CS_2 taken with 45 fs pulses, in 10% contours relative to the 2-D signal maximum. For comparison with the broad bandwidth data in Fig. 3, the Region II data should be inverted about the $t_2 = 0$ axis. (b) Semi-log plot of a slice of the 2-D signal $R^{(3)}(\tau_4)\cdot R^{(5)}(\tau_2,\tau_4)$ along τ_2 with $\tau_4 = 100$ fs. Lines show the decay times expected for a heterodyne (1.6 ps) and homodyne (0.8 ps) response. The small deviation from a 1.6 ps decay is expected for times < 2 ps. (c) Fifth order signal intensity as a function of the sum total incident intensity in all 4 beams taken at $\tau_2 = \tau_4 = 150$ fs. The arrow marks the intensity at which the data were taken.

the linear polarization directions of the i time ordered fields in the four-wave mixing process. This geometry limits the third order tensor component to be measured to the dynamics of the depolarized Raman spectrum. Note that as shown in Fig. 2 above, if the signal or dynamic range is large enough, no attenuation of the local oscillator is required, and the polarized spectrum can be measured ($\varphi_i = 0°$). The same geometries can be used in the intrinsically heterodyned fifth order signal. The polarized spectrum dynamics are observed by keeping all polarizations parallel ($\varphi_i = 0°$), as demonstrated here. Analysis of the fifth order tensor components [21] can lead to a geometry in which the fifth order signal is generated with its polarization crossed to the heterodyning third order signal field. A geometry that meets these requirements, and thus allows the magnitude of the local oscillator to be varied with the analyzing polarizer is $\varphi_1 = \varphi_2 = \varphi_5 = 0°$; $\varphi_3 = \varphi_4 = 45°$; $\varphi_6 = 90°$.

The shape of the 2-D response for small τ_2 and the features that define the ridge along the τ_4 variable are rather important in the simulation of the microscopic intermolecular liquid dynamics [9]. When trying to simulate a distribution of microscopic dynamics in the fifth order response, echo formation phenomena are expected both along the diagonal ($\tau_2 = \tau_4$) as well as along $\tau_2 = 0$ [1–3]. Also, simulations of fifth order response from anharmonic intermolecular modes show that the early portion of the τ_2 time scale is sensitive to the magnitude of the cubic anharmonicity [12]. An important distinction between the variable bandwidth data sets, and also the 60 fs homodyne results in Ref. [9], is the form of the decay along τ_4 for small τ_2. Whereas the long time behavior along the τ_2 axis is very similar between each data set (allowing for the hetero- or homodyne detection), the magnitude and shape of the ridge along τ_4 changes as a function of the detection bandwidth. A τ_4 ridge is quite obvious in the 27 fs data and disappears as the pulse width lengthens. This result can be understood qualitatively in terms of a number of observations. First, the symmetric nature of the signal depicted in Fig. 1c and Fig. 4a indicates that pulse width convolution effects will be far more dramatic for the response at small τ_4 than at small τ_2. In this region, the contours of the signal will be dictated by the superposition of the responses from Region I, Region II, and the $\tau_2 = 0$ hyperpolarizability signal. This is in addition to narrow bandwidth spectral filtering effects, which in 1-D measurements broaden and push back the inertial response of the liquid [27]. A true calculation of these bandwidth effects requires a summation over numerous Liouville space pathways [14] weighted by the spectral bandwidth. This is expected to have a significant effect on the fifth order signal, because a three level system is required in the description of the signal generation. Much of the simulation of fifth order signals thus far assumes infinite bandwidth and an infinite level harmonic oscillator coupled to a bath [1], which cannot capture interference effects with finite pulses at delay times comparable to the pulse width. All of the statements made here suggest that until these issues can be resolved more precisely, a broader bandwidth measurement is more reliable for comparison to the existing theories for the experiment.

The techniques demonstrated here suggest the possibility of using 2-D vibrational techniques as a probe of structure and dynamics in condensed phase molecular systems. Two-dimensional spectroscopy has been widely developed in the field of nuclear magnetic resonance to separate congested spectra in complex systems, probe couplings between spins, and address dynamic relationships between spectral features [25]. In principle, the bandwidths of fs pulses allow multidimensional Raman experiments to probe similar issues in the vibrational regime between 1 and 1000 cm^{-1}. The heterodyne technique presented here for fifth order Raman spectroscopy is general in that the same optical principles can be applied to a wide range of higher order resonant or nonresonant Raman experiments. The sensitivity of this method will allow 2-D measurements to be made even on weak Raman transitions.

Acknowledgements

This work was supported by a grant from the National Science Foundation. AT thanks the National Science Foundation for a Postdoctoral Research Fellowship. MJL and DSL are GAAN fellows.

References

[1] Y. Tanimura, S. Mukamel, J. Chem. Phys. 99 (1993) 9496.
[2] V. Khidekel, S. Mukamel, Chem. Phys. Lett. 240 (1995) 304.
[3] V. Khidekel, V. Chernyak, S. Mukamel, J. Chem. Phys. 105 (1996) 8543.
[4] K. Tominaga, K. Yoshihara, Phys. Rev. Lett. 171 (1995) 179.
[5] K. Tominaga, G.P. Keogh, Y. Naitoh, K. Yoshihara, J. Raman Spectrosc. 26 (1995) 495.
[6] K. Tominaga, K. Yoshihara, J. Chem. Phys. 104 (1996) 4419.
[7] T. Steffen, K. Duppen, Phys. Rev. Lett. 76 (1996) 1224.
[8] T. Steffen, K. Duppen, J. Chem. Phys. 106 (1997) 3854.
[9] A. Tokmakoff, G.R. Fleming, J. Chem. Phys. 106 (1997) 2569.
[10] K. Tominaga, K. Yoshihara, J. Chem. Phys. 104 (1996) 1159.
[11] K. Okumura, Y. Tanimura, J. Chem. Phys. 106 (1997) 1687.
[12] K. Okumura, Y. Tanimura, J. Chem. Phys. (1997) in press.
[13] K. Tominaga, K. Yoshihara, Phys. Rev. A 55 (1996) 831.
[14] T. Steffen, J.T. Fourkas, K. Duppen, J. Chem. Phys. 105 (1996) 7364.
[15] M.D. Levenson, S.S. Kano, Introduction to Nonlinear Laser Spectroscopy, Academic Press, Boston, MA, 1988.
[16] S. Mukamel, Principles of Nonlinear Optical Spectroscopy, Oxford University Press, New York, 1995.
[17] S. Matsuo, T. Tahara, Chem. Phys. Lett. 264 (1997) 636.
[18] P. Cong, Y.J. Chang, J.D. Simon, J. Phys. Chem. 100 (1996) 8613.
[19] Y.J. Chang, P. Cong, J.D. Simon, J. Chem. Phys. (1997) submitted.
[20] P. Vöhringer, N.F. Scherer, J. Phys. Chem. 99 (1995) 2684.
[21] A. Tokmakoff, J. Chem. Phys. 105 (1996) 13.
[22] M.S. Pshenichnikov, W.P. de Boeij, D.A. Wiersma, Opt. Lett. 19 (1994) 572.
[23] T. Joo, Y. Jia, G.R. Fleming, Opt. Lett. 20 (1995) 389.
[24] D. McMorrow, N. Thantu, J.S. Melinger, S.K. Kim, W.T. Lotshaw, J. Phys. Chem. 100 (1996) 10389.
[25] R.R. Ernst, G. Bodenhausen, A. Wokaun, Principles of Nuclear Magnetic Resonance in One and Two Dimensions, Oxford University Press, Oxford, 1987.
[26] D. McMorrow, W.T. Lotshaw, J. Phys. Chem. 95 (1991) 10395.
[27] D. McMorrow, W.T. Lotshaw, Chem. Phys. Lett. 174 (1990) 85.